Inorganic Chemistry

Article

pubs.acs.org/IC

Isolation and Crystallographic Characterization of Sm@C_{2v}(3)-C_{80} Through Cocrystal Formation with Ni^{II}(octaethylporphyrin) or Bis(ethylenedithio)tetrathiafulvalene

Hua Yang,[†] Zhimin Wang,[‡] Hongxiao Jin,[†] Bo Hong,[†] Ziyang Liu,*[,†] Christine M. Beavers,[§] Marilyn M. Olmstead,*[,∥] and Alan L. Balch*[,∥]

[†]College of Materials Science and Engineering, China Jiliang University, Hangzhou 310018, China

[‡]College of Biology and Environmental Engineering, Zhejiang Shuren University, Hangzhou, 310015, China

[§]Advanced Light Source, Lawrence Berkeley National Laboratory, One Cyclotron Road, Berkeley, California 94720, United States

[∥]Department of Chemistry, University of California, One Shields Avenue, Davis, California 95616, United States

Supporting Information

ABSTRACT: Sm@C_{2v}(3)-C_{80} has been separated from the carbon soot produced by electrical arc vaporization of graphite rods doped with Sm_2O_3 and purified. Its structure has been determined by single crystal X-ray diffraction using cocrystals obtained from either Ni^{II}(octaethylporphyrin) (Ni^{II}(OEP)) to form Sm@C_{2v}(3)-C_{80}·Ni^{II}(OEP)·1.68(toluene)·0.32(benzene) or bis(ethylenedithio)-tetrathiafulvalene (ET) to produce Sm@C_{2v}(3)-C_{80}·ET·0.5(toluene). Thus, this study offers the first opportunity to compare a common endohedral fullerene in two different cocrystals. Both cocrystals provide consistent information on the basic structure of Sm@C_{2v}(3)-C_{80} but show that the distribution of samarium ion sites inside the carbon cage depends upon whether Ni^{II}(OEP) or ET is present. The samarium ion is disordered in both structures, but the prominent sites lie slightly off the 2-fold symmetry axis of the cage. Computational studies at the B3LYP level indicate that Sm@C_{2v}(3)-C_{80} is more stable than any of the other six isomers of Sm@C_{80} that obey the isolated pentagon rule (IPR). The surface electrostatic potential of the interacting components in the cocrystals has been examined to identify factors responsible for the ordering of the fullerene cages. The regions of the Ni^{II}(OEP) or ET molecules that are closest to the fullerene display negative potential, while the corresponding regions of the endohedral fullerene show positive potential in a consistent fashion in both cocrystals.

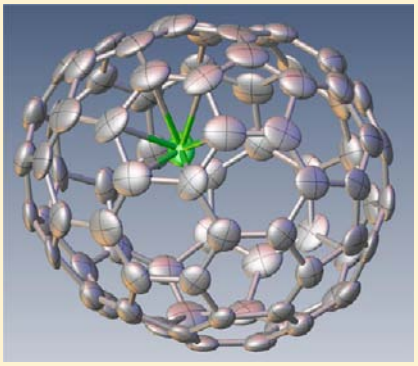

INTRODUCTION

The isolation and structural identification of $Sc_3N@I_h$-C_{80}, the third most abundant fullerene after the empty cages C_{60} and C_{70}, ushered in a new era in fullerene chemistry.[1] $Sc_3N@I_h$-C_{80} was the first endohedral fullerene to be characterized by single crystal X-ray diffraction. The high symmetry of many fullerene cages makes crystallographic studies difficult because of the presence of various sorts of orientational disorder.[2−4] Cocrystallization of fullerenes with a metalloporphyrin such as Ni^{II}(OEP) (OEP is the dianion of octaethylporphyrin, see Scheme 1) has been shown to produce crystals with sufficient order to allow structure determination.[5] This procedure has been used in our laboratory[6−9] and adopted by a number of other laboratories worldwide as a means to obtain structural information on empty cage fullerenes and endohedral fullerenes.[10−14]

The discovery of $Sc_3N@I_h$-C_{80} focused attention on the highly symmetric I_h-C_{80} cage. For example, molecules of the type $M_3N@I_h$-C_{80} have been prepared and isolated for M = Sc, Y, Gd, Tb, Dy, Ho, Er, Tm, and Lu.[15] Many mixed metal analogues, such as $CeSc_2N@I_h$-C_{80},[16] $ScGd_2N@I_h$-C_{80},[17] $Sc_2GdN@I_h$-C_{80}, and $TiSc_2N@I_h$-C_{80}[18] have been prepared, isolated, and

Scheme 1. Cocrystallization Agents

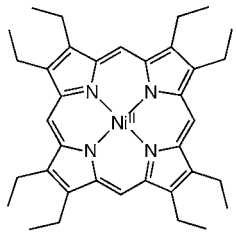

Ni^{II}(OEP)

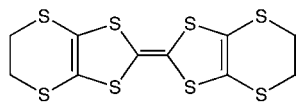

ET

structurally characterized. The I_h-C_{80} cage can also enclose other clusters including $Sc_4O_2@I_h$-C_{80},[19] $Sc_4O_3@I_h$-C_{80}, and $Sc_3C_2@I_h$-C_{80}.[20] Additionally, $La_2@I_h$-C_{80} and related dimetallic endohedrals utilize this I_h-C_{80} cage.[21,22] However, along with I_h-C_{80}, there are six other C_{80} isomers that satisfy the isolated pentagon rule (IPR), which requires that there are no pentagon-pentagon contacts in the fullerene and minimizes strain within

Received: August 15, 2012
Published: January 23, 2013

   dx.doi.org/10.1021/ic301794r | Inorg. Chem. 2013, 52, 1275−1284

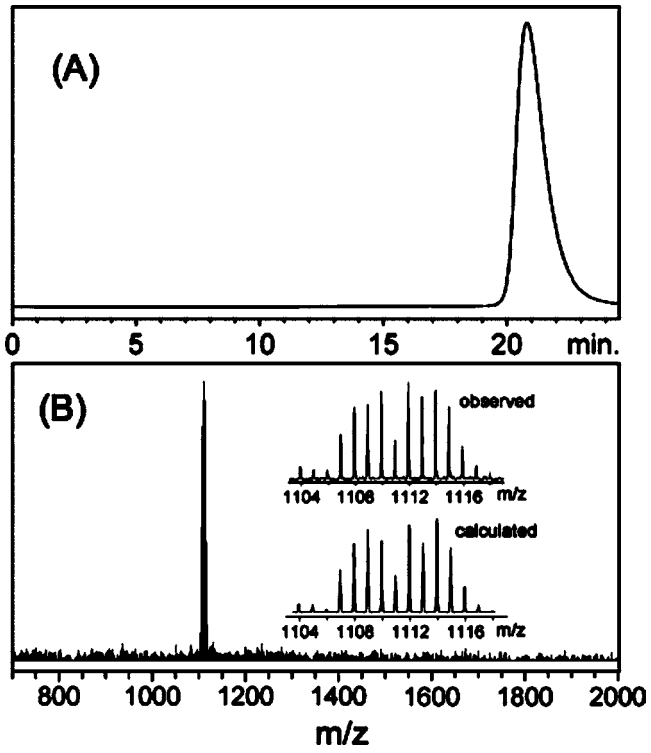

Figure 1. (**A**) Chromatogram of the purified Sm@C_{80} on a Buckyprep column (upper). The HPLC conditions are: flow rate 4.0 mL/min, detecting wavelength of 450 nm, eluent—toluene. (**B**) The LDI-TOF mass spectrum of the purified Sm@C_{80}. The insets show expansions of the observed and calculated spectra.

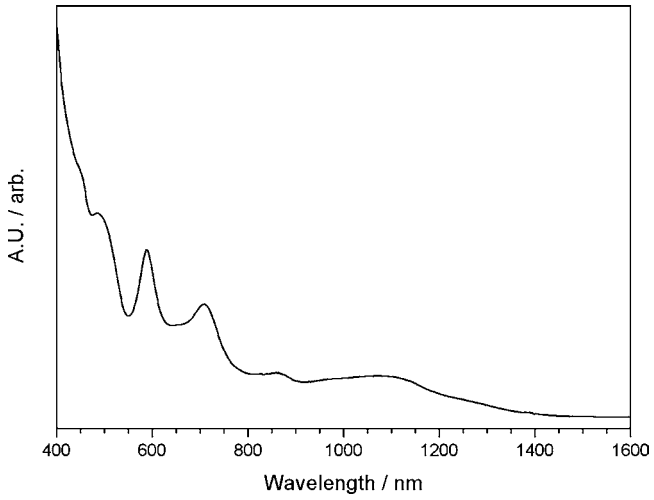

Figure 2. UV—vis—NIR absorption spectrum from a carbon disulfide solution of the purified isomer of Sm@C_{80}.

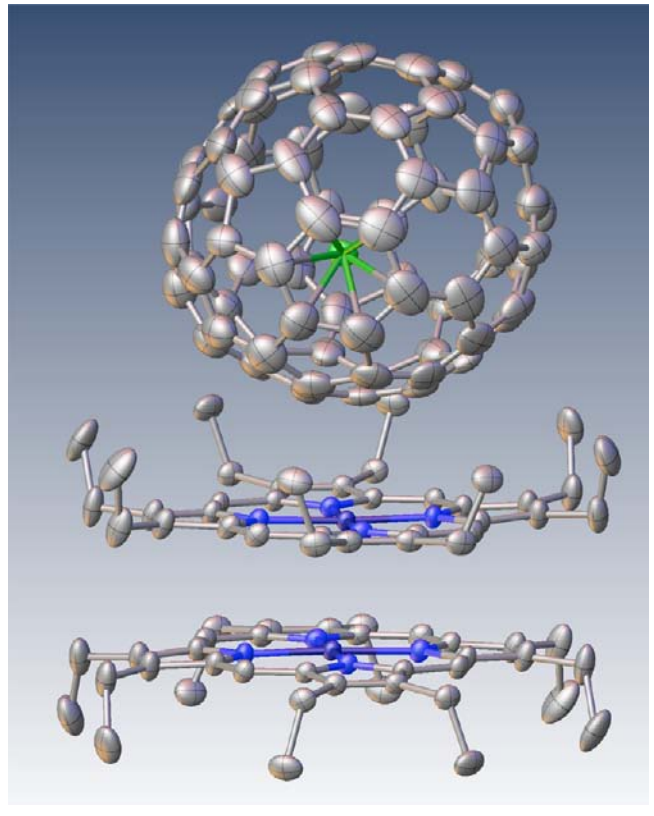

Figure 3. Drawing showing the interaction between the fullerene and porphyrin in Sm@$C_{2v}(3)$-C_{80}·Ni^{II}(OEP)·1.68(toluene)·0.32(benzene) with 50% thermal ellipsoids. Atom colors: Sm, green; C, gray; N, blue; Ni, violet. Only the major orientation of the fullerene cage and the major samarium ion site are shown. For clarity, hydrogen atoms and solvate molecules are not shown.

the fullerene cage by avoiding such contact between pentagons.[23] Many of these C_{80} isomers have been detected and structurally characterized. For empty cage C_{80}, three isomers have been observed: D_{5d}-C_{80},[24] D_2-C_{80},[25] and $C_{2v}(5)$-C_{80}.[26] For molecules of the $M_3N@C_{80}$ class, the $M_3N@D_{5h}$-C_{80} isomer also forms, albeit in lower yield, along with the $M_3N@I_h$-C_{80} isomer.[27] For $Dy_3N@C_{80}$, a third isomer, believed to be $Dy_3N@D_{5d}$-C_{80}, has been reported.[28] The $C_{2v}(5)$-C_{80} cage has been found in the carbide-containing endohedral fullerene, $Sc_2C_2@C_{2v}(5)$-C_{80}.[29] Recent work has shown that another C_{80} isomer is utilized in the monometallic endohedral fullerene, La@$C_{2v}(3)$-C_{80}.[30] La@$C_{2v}(3)$-C_{80} is one of the "missing metallofullerenes" that are found in the soot generated during conventional electric arc synthesis of fullerenes but cannot be extracted by most organic solvents. These "missing metallofullerenes" are likely to be polymerized in some fashion, but dissolve upon treatment with 1,2,4-trichlorobenzene. Solubilization is accomplished by addition of a dichlorophenyl group onto the endohedral fullerene. In contrast, Yb@$C_{2v}(3)$-C_{80} is a soluble endohedral fullerene that has been isolated in pristine form without the need for functionalization.[11]

The difference in behavior and reactivity between La@$C_{2v}(3)$-C_{80} and Yb@$C_{2v}(3)$-C_{80} may be attributed to the degree of electron transfer between the entrapped metal and the carbon cage. The metal atoms inside endohedral fullerenes are electropositive and transfer some of their electrons to the carbon cage.[31,32] With La (as with Ce, Pr, Nd, Gd, Tb, Dy, Ho, Er, and Lu) the metals adopt their usual 3+ oxidation state, and three electrons are transferred to the cage to produce the electronic distribution $M^{3+}@(C_{2n})^{3-}$. However, with endohedral fullerenes containing ytterbium (as well as Sm, Eu, Tm, Ca, Ba and Sr) only two electrons are transferred to the cage to form an electronic distribution of $M^{2+}@(C_{2n})^{2-}$. The cage reactivity reflects this electron transfer, which in the case of lanthanum, places three electrons on the cage and thus generates free radical-like characterisics.

Here, we report on the isolation and structural characterization of Sm@C_{80}. Unlike the situation with other endohedrals of the

dx.doi.org/10.1021/ic301794r | Inorg. Chem. 2013, 52, 1275−1284

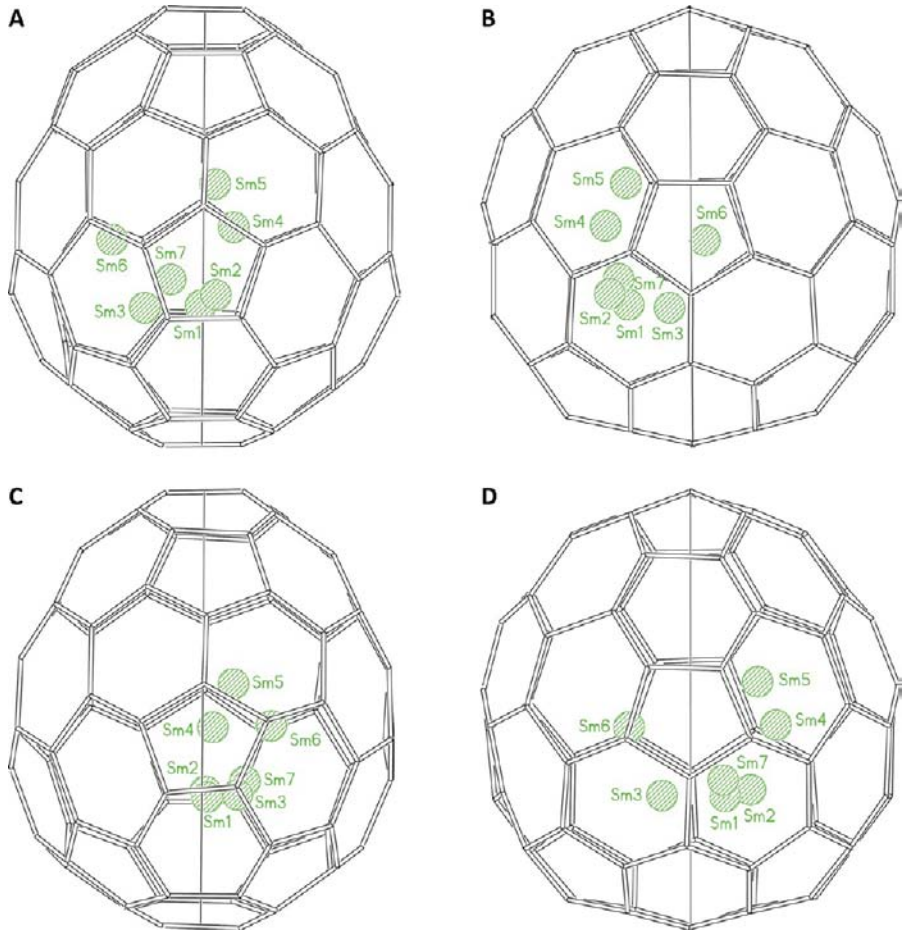

Figure 4. Pairs of orthogonal drawings showing the samarium ion positions in Sm@C_{2v}(3)-C_{80}·Ni^{II}(OEP)·1.68(toluene)·0.32(benzene); A and B, major cage orientation, C and D, minor cage orientation. The vertical line is the C_2 axis of the fullerene cage.

type Sm@C_{2n}, where several different isomers exist (e.g., four for Sm@C_{90},[33] five for Sm@C_{84}[34]) only one isomer of Sm@C_{80} has been reported previously.[35,36] To examine the structure of Sm@C_{80} in detail, we have used cocrystallization to obtain suitably diffracting material, but we have extended the cocrystallization procedure to include not only cocrystallization with Ni^{II}(OEP) but also with bis(ethylenedithio)tetrathiafulvalene (ET, which is sometimes called BEDT-TTF) (see Scheme 1). ET is an electron donor that has been shown to cocrystallize with C_{60},[37−39] but has not previously been used to form cocrystals with endohedral fullerenes.

RESULTS

Isolation of Sm@C_{80}. This endohedral fullerene was obtained from the carbon soot generated from the electric arc vaporization of a graphite rod filled with Sm_2O_3 and graphite powder.[17,40,41] The carbon soot was extracted with *o*-dichlorobenzene, which readily dissolves fullerenes in the carbon soot. After concentration, the soluble extract was subjected to a five-stage, high pressure liquid chromatographic (HPLC) isolation process involving initially a Buckyprep-M column with a chlorobenzene mobile phase to maximize the efficiency of this step, then a Buckyprep column with toluene as eluent, a 5PBB column with chlorobenzene as eluent, a Buckyprep-M column with toluene as eluent and finally a Buckyprep column with toluene as eluent. A single isomer of Sm@C_{80} was obtained. Figure 1 shows the HPLC chromatogram and the mass spectrum of the purified sample.

Figure 2 shows the UV−vis−NIR absorption spectrum of Sm@C_{80}. The onset of absorption occurs at 1400 nm. Absorption maxima occur at 1079, 862, 708, 590, 490, and 454 nm. The spectrum is similar to the one reported earlier for the single isomer of Sm@C_{80} obtained by T. Okazaki et al.[35,36] Consequently, it appears that both laboratories produced the same isomer of Sm@C_{80}, although different sources of samarium were used in the two laboratories. Okazaki et al. used the Sm_2Co_{17} alloy as their samarium source,[35,36] whereas we used Sm_2O_3. In contrast, for Sm@C_{84} and for Sm@C_{82}, the chemical source of the samarium affected the array of isomers produced.[35,42] The UV−vis−NIR absorption spectrum of Sm@C_{80} is also similar to those reported for Yb@C_{2v}(3)-C_{80},[31] Ca@C_{80},[43] Ba@C_{80}, Sr@C_{80}, and Eu@C_{80}.[44] Thus, these M^{2+}@$(C_{2n})^{2-}$ endohedral fullerenes utilize the same fullerene cage, since the UV−vis−NIR absorption spectra of endohedral fullerenes are determined by the isomeric structure of the cage.

Crystallographic Characterization of Sm@C_{2v}(3)-C_{80}·Ni^{II}(OEP)·1.68(Toluene)·0.32(Benzene). The endohedral fullerene in benzene solution was cocrystallized with Ni^{II}(OEP) in toluene solution to form black crystals of Sm@C_{2v}(3)-C_{80}·Ni^{II}(OEP)·1.68(toluene)0.32(benzene). Figure 3 shows the orientation of the Sm@C_{2v}(3)-C_{80} molecule with regard to the adjacent nickel porphyrin. This drawing also includes a second Ni^{II}(OEP) molecule to show the back-to-back arrangement of these two porphyrins. Such back-to-back contact between

dx.doi.org/10.1021/ic301794r | *Inorg. Chem.* 2013, 52, 1275−1284

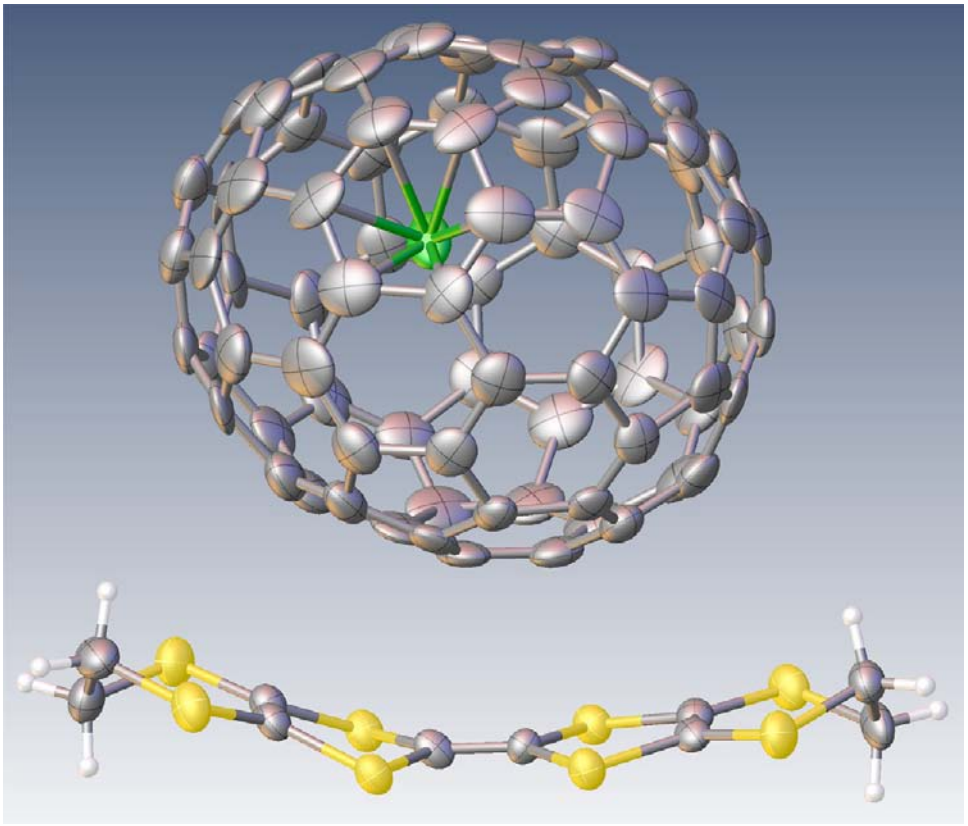

Figure 5. Drawing showing the interaction between the fullerene and the ET molecule in Sm@C_{2v}(3)-C_{80}·ET·0.5(toluene) with 50% thermal ellipsoids. Atom colors: Sm, green; C, gray; S, yellow: H, white. Only the major orientation of the fullerene cage and the position of Sm1 are shown. For clarity toluene molecules, the second orientation of the fullerene cage, and three other samarium sites are omitted.

porphyrins is a feature found in many cocrystals of fullerenes and endohedral fullerenes with Ni^{II}(OEP) or Co^{II}(OEP). There are two orientations of the C_{80} cage in the crystal. Figure 3 shows only the major orientation, which has 0.556(3) occupancy. Although there are seven sites for the samarium ion inside the cage, only the most populated site (Sm1, 0.37 fractional occupancy) is shown in Figure 3.

Figure 4 shows drawings of the Sm@C_{2v}(3)-C_{80} molecule itself in Sm@C_{2v}(3)-C_{80}·Ni^{II}(OEP)·1.68(toluene)0.32-(benzene) with the 2-fold axis aligned vertically. The positions of all seven of the samarium ion sites (fractional occupancies: Sm1, 0.37; Sm2, 0.24; Sm3, 0.19: Sm4, 0.06; Sm5, 0.04; Sm6, 0.04; Sm7, 0,04) are shown for the two different orientations of the cage. The seven samarium ion positions lie near a plane that is nearly parallel to the plane of the neighboring Ni^{II}(OEP) molecule. They form a crescent that follows the contours of the widest part of the C_{2v}(3)-C_{80} cage. Sm1 lies in an off-center position near a hexagonal face of the fullerene for both orientations of the cage. This location for the samarium ion is shown in Figure 3 for the major orientation of the cage. However, this view of the structure is somewhat misleading. Sm2 and Sm3, each with significant occupancies, are found in different environments. Both of these ions lie over the 6:6 ring junctions at the center of a pyracylene patch on the fullerene and are, in general, closer to individual carbon atoms in the cage than is Sm1.

Crystallographic Characterization of Sm@C_{2v}(3)-C_{80}·ET·0.5(Toluene). Cocrystallization of Sm@C_{2v}(3)-C_{80} with ET in toluene solution produced black crystals of Sm@C_{2v}(3)-C_{80}·ET·0.5(toluene). Figure 5 shows a drawing of the Sm@C_{2v}(3)-C_{80} molecule and its orientation relative to a ET molecule. Comparisons of Figures 3 and 5 show that the fullerene cages are similarly situated over the relatively flat portions of the Ni^{II}(OEP) and ET molecules in the two different cocrystals.

The C_{80} cage has two different orientations in the crystal: the major one with 0.583(4) fractional occupancy and a minor one with 0.417(4) occupancy. Only the major cage site is shown in Figure 5. There are also four sites for the samarium ion with fractional occupancies of 0.332(3) for Sm1, 0.2960(16) for Sm2, 0.243(2) for Sm3, and 0.129(4) for Sm4. Only Sm1, which is located near the center of a hexagon, is shown in Figure 5. This location involves the same hexagonal ring that is close to Sm1 in the Ni^{II}(OEP) cocrystal. In that regard the two cocrystals are quite similar. However, when all of the samarium ion positions in both orientations of the fullerene cage are considered, a more complicated situation is observed.

Figure 6 shows drawings of the C_{2v}(3)-C_{80} cage in the ET cocrystal with the 2-fold axis aligned vertically. The locations of the four samarium ion sites inside are also shown. The samarium ions interact with the cage in a wide variety of ways. Sm1 is near the center of a hexagon in the major cage orientation, while it lies well off to the side of a hexagon near only three carbon atoms in the minor cage orientation. Sm2 lies near the center of a pyracylene patch in the major cage orientation but lies over a 5:6 ring junction in the minor cage orientation. Sm3 lies in a slightly off-center position over a hexagon in the major cage orientation but over a pyracylene patch in the minor cage orientation. Sm4 lies over a pentagon in both cage orientations. Since the samarium ion occupies such an array of sites, it seems that the samarium ion must be fairly free to move about the C_{2v}(3)-C_{80} cage.

dx.doi.org/10.1021/ic301794r | *Inorg. Chem.* 2013, 52, 1275−1284

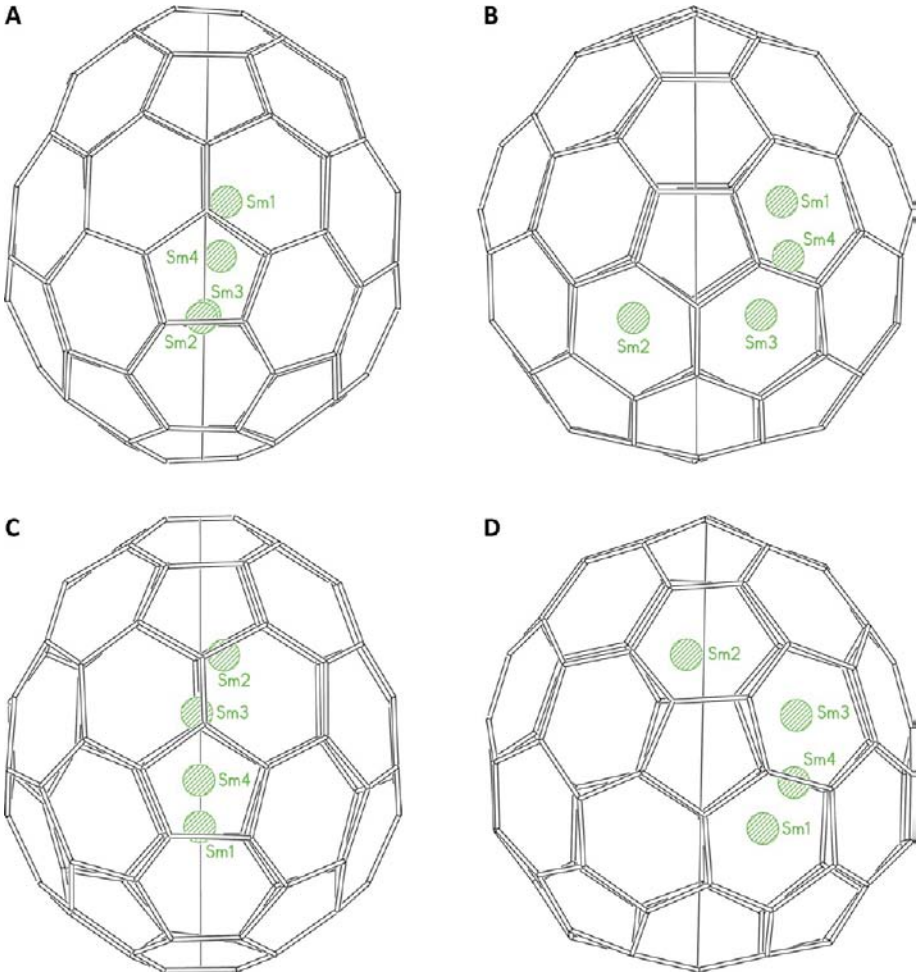

Figure 6. Pairs of orthogonal drawings showing the samarium ion positions in Sm@C_{2v}(3)-C_{80}·ET·0.5(toluene); A and B, major cage orientation, C and D, minor cage orientation. The vertical line is the C_2 axis of the fullerene cage.

As seen in Figure 5, the inner C_6S_8 unit of the ET molecule is not planar. Rather there is bending at the inner set of four sulfur atoms that allows the shape of the ET molecule to conform to that of the nearby C_{2v}(3)-C_{80} cage. ET is known to be flexible in that regard. Both planar[45] and curved[46] structures have been observed for neutral ET in various cocrystals. Since there are two locations for the C_{80} cage, there are two ways that cage can overlap with the ET molecule. Those two different patterns of overlap are shown in Figure 7.

The ET molecules do not participate in the back-to-back packing that is characteristic of cocrystals of fullerenes and Ni^{II}(OEP). As an alternative, each ET molecule makes contacts with four neighboring Sm@C_{2v}(3)-C_{80} molecules, as can be seen in the stereo drawing shown in Figure 8. Only the major orientation of the Sm@C_{2v}(3)-C_{80} molecule is shown here. The dashed lines in Figure 8 show the close approaches of the sulfur atoms of the ET molecule with carbon atoms in the nearby endohedral fullerenes. For the major orientation shown, the shortest of the S···C contact between ET and an endohedral is 3.317 Å. For the minor orientation, the closest S···C contact is even shorter, 3.145 Å.

Computational Studies of the Isomeric C_{80} Cages. To further understand the electronic and geometric structures of the C_{80} isomers, geometric optimizations using density functional theory (DFT) methodology were conducted for the seven Sm@C_{80} isomers that obey the IPR. The relative energies and gaps between the highest occupied molecular orbital (HOMO) and the lowest unoccupied molecular orbital (LUMO) for these isomers are presented in Table 1. Sm@C_{2v}(3)-C_{80} is the most stable of these isomers and also possesses the largest HOMO−LUMO gap. We have also explored the positioning of the Sm ion inside the fullerene cage. The potential well along the interior fullerene surface is shallow, but the global minimum places the samarium ion beneath a hexagonal ring as shown in Figures 3 and 5, a position that corresponds to the major samarium site, Sm1, in Sm@C_{2v}(3)-C_{80}·Ni^{II}(OEP)·1.68(toluene)·0.32(benzene).

The electronic distribution for samarium containing endohedral fullerenes may be represented by an ionic model, Sm^{2+}@$(C_{2n})^{2-}$, where the cage acquires two-electrons from the interior metal atom.[32,33] Figure 9 shows the molecular orbital energies computed for the neutral, di-, tri-, and tetra-anionic forms of the empty cage C_{2v}(3)-C_{80} using DFT methodology. The dianion has the largest HOMO−LUMO gap, which is frequently an indicator of isomer stability.

The computed structure and spin density distribution in Sm@C_{2v}(3)-C_{80} are shown in Figure 10. Additionally, this figure shows the calculated structure and spin density for La@C_{2v}(3)-C_{80}. This figure provides an explanation for the different reactivities of these two endohedrals. The spin density of La@C_{2v}(3)-C_{80} is wholly distributed on the carbon cage and contributes to the chemical reactivity for an endohedral with the electronic distribution La^{3+}@$(C_{80})^{3-}$. In contrast, the spin density of Sm@C_{2v}(3)-C_{80} is confined to the samarium ion and a few nearby

dx.doi.org/10.1021/ic301794r | Inorg. Chem. 2013, 52, 1275−1284

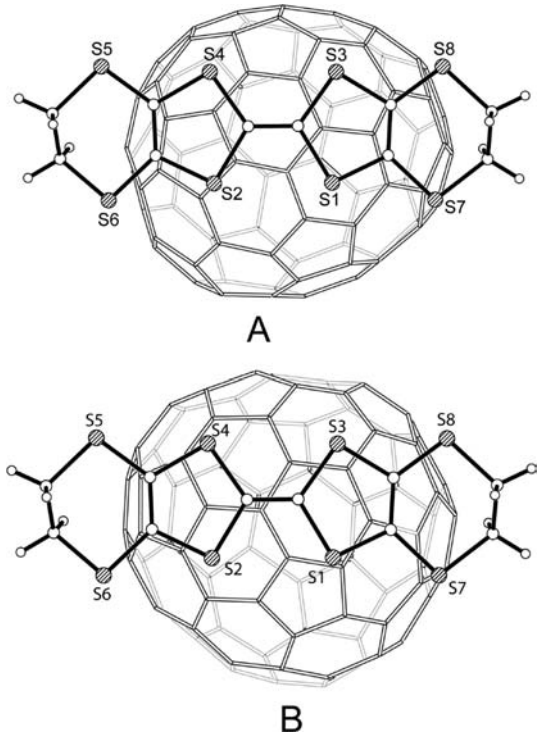

Figure 7. Drawing showing the orientation of the C_{80} cage and the facing ET molecule in Sm@C_{2v}(3)-C_{80}·ET·0.5(toluene). For clarity, the samarium ion positions are not shown. **A**, major cage orientation with 0.583(4) occupancy; **B**, minor cage orientation with 0.417(4) occupancy. Orientation **A** shows a close contact from S2 of ET to C55 of the fullerene of 3.328 Å. The shortest S···C contact for orientation B is S1···C22 at 3.602 Å .

carbon atoms. Consequently, La@C_{2v}(3)-C_{80} is a reactive, free radical like molecule, which has yet to be isolated in pristine form. In contrast, Sm@C_{2v}(3)-C_{80} has been isolated and has an ordinary closed shell cage with a paramagnetic metal ion shielded inside the cage.

The relative orientations of the individual molecules in cocrystals of fullerenes and endohedral fullerenes must result from a combination of factors. When the fullerene contains relatively flat regions, the relationship between the fullerene and the Ni^{II}(OEP) molecules appears in many cases to favor placing the flat region of the fullerene near the porphyrin plane. However, some notable exceptions have appeared: for example, La_2@D_5(450)-C_{100} where the curved poles of the fullerene are closest to the porphyrin.[47] Consequently, we have begun to examine other factors that might influence the relationship between molecules in

Table 1. Relative Energies and HOMO−LUMO Gaps of Sm@C_{80} Isomers Calculated at B3LYP (3-21g for C, CEP-31g for Sm) Level

isomers	ΔE, kcal·mol^{-1}	HOMO−LUMO gap, eV
Sm@C_{2v}(3)-C_{80}	0.000	1.71
Sm@C_{2v}(5)-C_{80}	6.170	1.16
Sm@D_{5h}(6)-C_{80}	9.260	1.32
Sm@D_{5d}(1)-C_{80}	11.634	1.56
Sm@D_3(4)-C_{80}	12.798	1.36
Sm@D_2(2)-C_{80}	19.796	1.53
Sm@I_h(7)-C_{80}	35.143	0.79

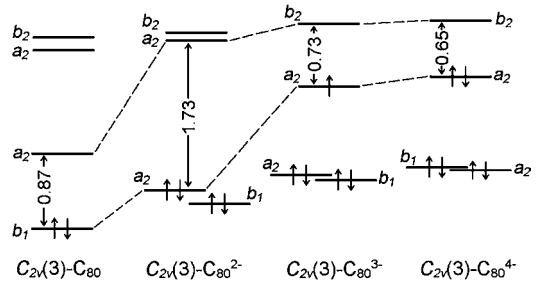

Figure 9. Molecular orbital energy levels (in eV) for the neutral form as well as di-, tri-, and tetra-anions of the empty C_{2v}(3)-C_{80} molecule. The calculations were conducted at the B3LYP/6-31G(d) level.

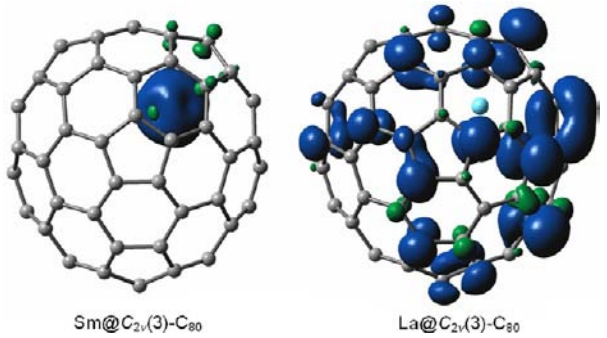

Figure 10. Computed structures and spin density distributions in Sm@C_{2v}(3)-C_{80} and La@C_{2v}(3)-C_{80} at the isovalue of 0.0006 e/Bohr^3.

fullerene-containing cocrystals. One of these factors is the surface electrostatic potential of the interacting components.[48,49]

Figure 11 presents plots of the electrostatic potential in terms of total electron density for the Sm@C_{2v}(3)-C_{80}·Ni^{II}(OEP) unit found in the crystals reported here. The regions of the porphyrin that are closest to the fullerene display negative potential (red coloration)

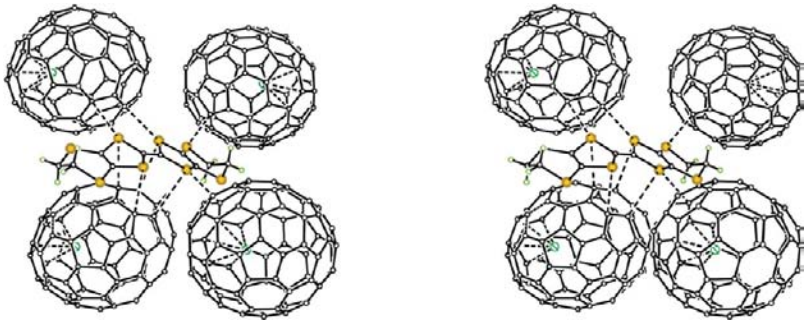

Figure 8. Stereo drawing showing the interactions between the Sm@C_{2v}(3)-C_{80} cage and the neighboring ET molecules in Sm@C_{2v}(3)-C_{80}·ET·0.5(toluene). Only the major samarium site and one orientation of the cage are shown.

dx.doi.org/10.1021/ic301794r | Inorg. Chem. 2013, 52, 1275−1284

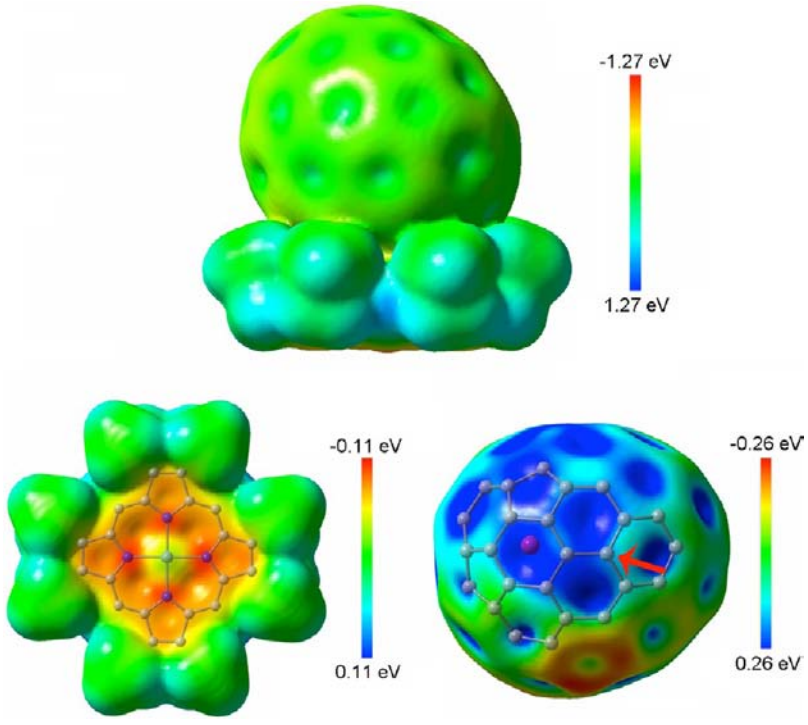

Figure 11. Plots of electrostatic potentials (in eV) mapped on the isosurfaces of the total electron densities (0.001 e/Bohr^3). Top: the entire complex Sm@C_{2v}(3)-C_{80}·Ni^{II}(OEP). Lower left, the surface of Ni^{II}(OEP) facing the Sm@C_{2v}(3)-C_{80} molecule. Lower right, the portion of Sm@C_{2v}(3)-C_{80} facing the Ni^{II}(OEP) molecule. Two-dimensional projections of the bonds onto the plots are also shown for clarity. The red arrow indicates the carbon atom nearest the nickel ion.

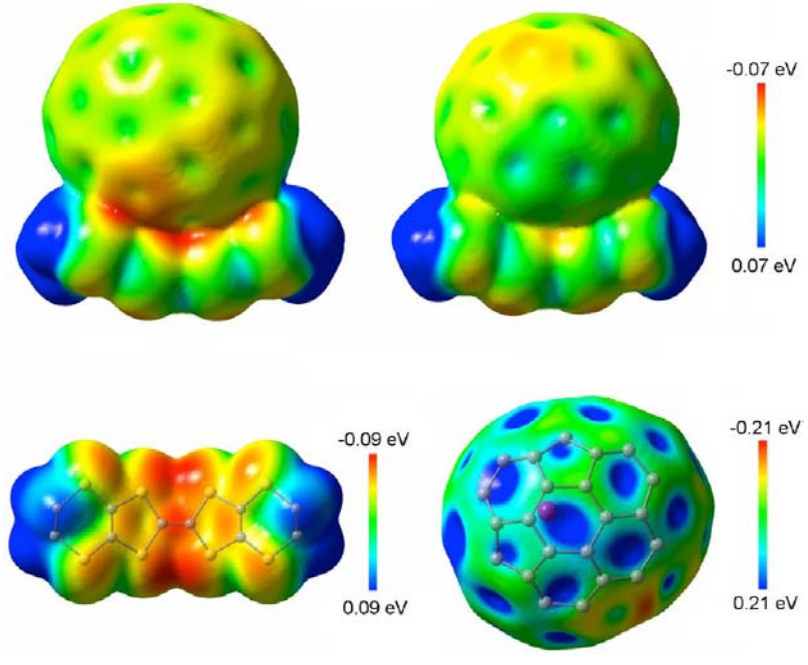

Figure 12. Plots of electrostatic potentials (in eV) mapped on the isosurfaces of total electron densities (0.001 e/Bohr^3). Top, the Sm@C_{2v}(3)-C_{80}·ET complex viewed from two sides. Lower left, the portion of the ET molecule facing the Sm@C_{2v}(3)-C_{80} molecule. Lower right, the part of Sm@C_{2v}(3)-C_{80} that faces the ET molecule. Two-dimensional projections of the bonds onto the plots are also shown for clarity.

in the vicinity of the four nitrogen atoms. On the other hand, the blue-green color in the regions of the endohedral fullerene that are close to the porphyrin indicates regions of significant positive potential. Thus, there is a complementarity of surface potentials in the regions of close contact between these two molecules.

Figure 12 presents similar plots of electrostatic potential for the Sm@C_{2v}(3)-C_{80}·ET unit found in Sm@C_{2v}(3)-C_{80}·ET·0.5(toluene). Again, the flat region of the ET molecule that faces the endohederal fullerene displays negative potential as indicated by the red color at the center of the molecule, while the part of the

dx.doi.org/10.1021/ic301794r | *Inorg. Chem.* 2013, 52, 1275−1284

endohedral fullerene nearby shows substantial positive potential. Overall, the electrostatic potentials shown in Figures 11 and 12 follow similar patterns.

DISCUSSION

This work has allowed us to identify the only isomer of Sm@C_{80} that forms as Sm@$C_{2v}(3)$-C_{80} and has given us the unusual opportunity to examine the structure of an endohedral fullerene in two different crystalline environments. Both cocrystals formed here show disorder in the positions of the fullerene cage and in the position of the samarium ion inside the cage. However, the basic geometry of the $C_{2v}(3)$-C_{80} cage is clear. As seen on Figures 4 and 6, the cage is slightly narrower when viewed from the perspective shown in parts A and C, while it is wider in the views B and D. Inside the cage, the samarium ion is distributed over a set of sites. In both cocrystals these sites lie nearly in a plane, but the sites are not equally distributed about the 2-fold axis in either cocrystal. Rather, they form a crescent that follows the curve of the wider portion of the fullerene cage. The samarium ion inside other endohedral fullerenes of the type Sm@C_{2n} is frequently found spread over a range of sites near the walls of the cages.[34,35] In this context it is interesting to compare and contrast the structures of the two $M^{2+}@(C_{2n})^{2-}$ type endohedrals: Sm@$C_{2v}(3)$-C_{80} and Yb@$C_{2v}(3)$-C_{80}. In Yb@$C_{2v}(3)$-C_{80}, the ytterbium ion basically has only one position, over a hexagon but off to the side of the 2-fold axis of the cage.[31] In both cocrystals of Sm@$C_{2v}(3)$-C_{80}, the position of Sm1 lies over the corresponding hexagon and to one side of the 2-fold axis. However, for the Sm@$C_{2v}(3)$-C_{80} cocrystals there are several alternative sites for the samarium ion that are partially occupied. It will be interesting to see whether there are other cases of metal ion dependent positioning of the internal contents as more and more endohedral fullerenes are crystallographically characterized.

It appears that the cocrystallizing molecule, Ni^{II}(OEP) or ET, exerts some influence on the location of the samarium ion inside the cage, since the distributions of samarium ion sites are different in the two cocrystals. Similarly, Ni^{II}(OEP) seems to induce the M_3N unit in cocrystals with $M_3N@I_h$-C_{80} into an orientation perpendicular to the porphyrin plane with two metal ions near the plane.[50]

The surface electrostatic potential of the interacting components in these cocrystals appears to play a role in inducing some degree of order in the location of the fullerene cages. The regions of Ni^{II}(OEP) or ET molecules that are closest to the fullerene display negative potential, while the corresponding regions of the endohedral fullerene show positive potential in a consistent fashion in both cocrystals.

EXPERIMENTAL SECTION

Formation and Isolation of Sm@C_{80}. An 8 × 150 mm graphite rod filled with Sm_2O_3 and graphite powder (Sm:C atomic ratio 1:40) was vaporized as the anode in a direct current (DC) arc discharge under optimized conditions. The raw soot was sonicated in *o*-dichlorobenzene for 8 h and then vacuum filtered. After removing the solvent with a rotary evaporator, chlorobenzene was added to redissolve the dry extract. The resulting solution was subjected to a five-stage HPLC isolation process without recycling. Chromatographic details are given in the Supporting Information.

The purity and composition of the sample of Sm@C_{80} were verified by laser desorption time-of-flight mass spectrometry (LD-TOF-MS). Ultraviolet−visible-near-infrared (UV−vis−NIR) spectra were obtained through the use of a UV-4100 spectrophotometer (Hitachi High-Technologies Corporation) with samples dissolved in carbon disulfide.

Crystal Growth. Black crystals of Sm@$C_{2v}(3)$-C_{80}·Ni^{II}(OEP)·1.68(toluene)·0.32(benzene) were obtained by the slow diffusion of solutions of Sm@$C_{2v}(3)$-C_{80} dissolved in benzene and of Ni^{II}(OEP) in toluene. Crystals of Sm@$C_{2v}(3)$-C80·ET·0.5(toluene) were obtained in a similar fashion in toluene solution from a purified sample of Sm@$C_{2v}(3)$-C_{80} and ET.

Crystal Structure Determinations. The black crystals of both compounds were mounted in the nitrogen cold stream provided by an Oxford Cryostream low temperature apparatus on the goniometer head of a Bruker D8 diffractometer equipped with an ApexII CCD detector at the Advanced Light Source, Berkeley, CA, beamline 11.3.1. Data were collected with the use of silicon(111) monochromated synchrotron radiation (λ = 0.77490 Å). Both data sets were reduced with the use of Bruker SAINT[51] and a multiscan absorption correction applied with the use of SADABS.[52] Crystal data are given in Table 2. The structures were solved by direct methods (SHELXS97) and refined by full-matrix least-squares on F^2 (SHELXL97).[53] Figures 3 and 5 were drawn using OLEX2.[54]

Table 2. Crystal Data and Data Collection Parameters

	Sm@$C_{2v}(3)$-C_{80}·Ni^{II}(OEP)·1.68(toluene)·0.32(benzene)	Sm@$C_{2v}(3)$-C_{80}·ET·0.5(toluene)
formula	$C_{129.68}H_{59.36}N_4NiSm$	$C_{93.5}H_{12}S_8Sm$
fw	1882.36	1541.86
color, habit	black block	black parallelepiped
crystal system	monoclinic	monoclinic
space group	$P2_1/c$	$P2_1/c$
a, Å	20.3181(7)	10.8264(6)
b, Å	14.7432(5)	21.5495(11)
c, Å	25.3393(8)	22.5795(11)
β, deg	96.408(2)	101.688(4)
V, Å^3	7543.1(4)	5158.6(5)
Z	4	4
T (K)	100(2)	100(2)
radiation (λ, Å)	synchrotron 0.77490	synchrotron 0.77490
unique data	27477 [*R*(int) = 0.0622]	11599 [*R*(int) = 0.075]
parameters	1946	1709
restraints	4170	3895
obsd ($I > 2\sigma(I)$) data	18445	9344
R1[a] (obsd data)	0.094	0.097
wR2[b] (all data)	0.313	0.259

[a]For data with $I > 2\sigma(I)$ $R1 = (\sum||F_o| - |F_c||)/(\sum|F_o|)$. [b]For all data. $wR2 = [\sum w(F_o^2 - F_c^2)^2/\sum w(F_o^2)^2]^{1/2}$.

Computational Details. Geometries the isomers of C_{80} were fully optimized by nonlocal density functional calculations at the B3LYP level.[55] The effective core potential and basis set developed by Stevens et al. were used for samarium (CEP-31g),[56] and the split-valence 3-21g basis set was used for carbon. All calculations were carried out with the GAUSSIAN 09 program.[57]

ASSOCIATED CONTENT

Supporting Information

Isolation procedures, computational details and X-ray crystallographic files in CIF format for Sm@$C_{2v}(3)$-C_{80}·Ni^{II}(OEP)·1.68(toluene)·0.32(benzene) and Sm@$C_{2v}(3)$-C_{80}·ET·0.5(toluene). This material is available free of charge via the Internet at http://pubs.acs.org.

AUTHOR INFORMATION

Corresponding Author

*E-mail: zyliu@zju.edu.cn (Z.L.), mmolmstead@ucdavis.edu (M.M.O.), albalch@ucdavis.edu (A.L.B.).

Notes

The authors declare no competing financial interest.

■ ACKNOWLEDGMENTS

We thank the U.S. National Science Foundation [Grant CHE-1011760 to A.L.B. and M.M.O.], the National Natural Science Foundation of China [21271162, 11274283, 11179039], the Natural Science Foundation of Zhejiang Province of China [R12B010002, Y4090430], and the Advanced Light Source, Lawrence Berkeley Laboratory, for support. The Advanced Light Source is supported by the Director, Office of Science, Office of Basic Energy Sciences, of the U.S. Department of Energy under Contract No. DE-AC02-05CH11231.

■ REFERENCES

(1) Stevenson, S.; Rice, G.; Glass, T.; Harich, K.; Cromer, F.; Jordan, M. R.; Craft, J.; Hadju, E.; Bible, R.; Olmstead, M. M.; Maitra, K.; Fisher, A. J.; Balch, A. L.; Dorn, H. C. *Nature* **1999**, *401*, 55.
(2) Heiney, P. A.; Fischer, J. E.; McGhie, A. R.; Romanow, W. J.; Denenstein, A. M.; McCauley, J. P.; Smith, A. B., Jr; Cox, D. E. *Phys. Rev. Lett.* **1991**, *66*, 2911.
(3) Bürgi, H. B.; Blanc, E.; Schwarzenbach, D.; Liu, S.; Lu, Y.-J.; Kappes, M. M.; Ibers, J. A. *Angew. Chem., Int. Ed. Engl.* **1992**, *31*, 640.
(4) Olmstead, M. M.; Balch, A. L.; Lee, H. M. *Acta Crystallogr., Sect. B: Struct. Sci.* **2012**, *B68*, 66.
(5) Olmstead, M. M.; Costa, D. A.; Maitra, K.; Noll, B. C.; Phillips, S. L.; Van Calcar, P. M.; Balch, A. L. *J. Am. Chem. Soc.* **1999**, *121*, 7090.
(6) Mercado, B. Q.; Jiang, A.; Yang, H.; Wang, Z.; Jin, H.; Liu, Z.; Olmstead, M. M.; Balch, A. L. *Angew. Chem., Int. Ed.* **2009**, *48*, 9114.
(7) Mercado, B. Q.; Olmstead, M. M.; Beavers, C. M.; Easterling, M. L.; Stevenson, S.; Mackey, M. A.; Coumbe, C. E.; Phillips, J. D.; Phillips, J. P.; Poblet, J. M.; Balch, A. L. *Chem. Commun.* **2010**, *46*, 279.
(8) Yang, H.; Beavers, C. M.; Wang, Z.; Jiang, A.; Liu, Z.; Jin, H.; Mercado, B. Q.; Olmstead, M. M.; Balch, A. L. *Angew. Chem., Int. Ed.* **2010**, *49*, 886.
(9) Beavers, C. M.; Jin, H.; Yang, H.; Wang, Z.; Wang, X.; Ge, H.; Liu, Z.; Mercado, B. Q.; Olmstead, M. M.; Balch, A. L. *J. Am. Chem. Soc.* **2011**, *133*, 15338.
(10) Yang, S. F.; Troyanov, S. I.; Popov, A. A.; Krause, M.; Dunsch, L. *J. Am. Chem. Soc.* **2006**, *128*, 16733.
(11) Lu, X.; Lian, Y.; Beavers, C. M.; Mizorogi, N.; Slanina, Z.; Nagase, S.; Akasaka, T. *J. Am. Chem. Soc.* **2011**, *133*, 10772.
(12) Kurihara, H.; Lu, X.; Iiduka, Y.; Nikawa, H.; Hachiya, M.; Mizorogi, N.; Slanina, Z.; Tsuchiya, T.; Nagase, S.; Akasaka, T. *Inorg. Chem.* **2012**, *51*, 746.
(13) Epple, L.; Amsharov, K. Yu.; Jansen, M. *Fullerenes, Nanotubes, Carbon Nanostruct.* **2009**, *17*, 67.
(14) Ziegler, K.; Amsharov, K. Yu.; Halasz, I.; Jansen, M. *Z. Anorg. Allg. Chem.* **2011**, *637*, 1463.
(15) Dunsch, L.; Yang, S. F. *Small* **2007**, *3*, 1298.
(16) Wang, X.; Zuo, T.; Olmstead, M. M.; Duchamp, J. C.; Glass, T. E.; Cromer, T. E.; Balch, A. L.; Dorn, H. C. *J. Am. Chem. Soc.* **2006**, *128*, 8884.
(17) Stevenson, S.; Chancellor, C. J.; Lee, H. M.; Olmstead, M. M.; Balch, A. L. *Inorg. Chem.* **2008**, *47*, 1420.
(18) Yang, S. F.; Chen, C.; Popov, A. A.; Zhang, W.; Liu, F.; Dunsch, L. *Chem. Commun.* **2009**, 6391.
(19) Stevenson, S.; Mackey, M. A.; Stuart, M. A.; Phillips, J. P.; Easterling, M. L.; Chancellor, C. J.; Olmstead, M. M.; Balch, A. L. *J. Am. Chem. Soc.* **2008**, *130*, 11844.
(20) Iiduka, Y.; Wakahara, T.; Nakahodo, T.; Tsuchiya, T.; Sakuraba, A.; Maeda, Y.; Akasaka, T.; Yoza, K.; Horn, E.; Kato, T.; Liu, M. T. H.; Mizorogi, N.; Kobayashi, K.; Nagase, S. *J. Am. Chem. Soc.* **2005**, *127*, 12500.
(21) Suzuki, T.; Maruyama, Y.; Kato, T.; Kikuchi, K.; Nakao, Y.; Achiba, Y.; Kobayashi, K.; Nagase, S. *Angew. Chem., Int. Ed. Engl.* **1995**, *34*, 1094.
(22) Shimotani, H.; Ito, T.; Iwasa, Y.; Taninaka, A.; Shinohara, H.; Nishibori, E.; Takata, M.; Sakata, M. *J. Am. Chem. Soc.* **2004**, *126*, 364.
(23) Fowler, P. W.; Manolopoulous, D. E. *An Atlas of Fullerenes*; Clarendon: Oxford, U.K., 1995.
(24) Hennrich, F. R.; Michel, R. H.; Fischer, A.; Richard-Schneider, S.; Gilb, S.; Kappes, M. M.; Fuchs, D.; Burk, M.; Kobayashi, K.; Nagase, S. *Angew. Chem., Int. Ed. Engl.* **1996**, *35*, 1732.
(25) Wang, C.-R.; Sugai, T.; Kai, T.; Tomiyhama, T.; Shinohara, H. *Chem. Commun.* **2000**, 557.
(26) Shustova, N. B.; Kuvychko, I. V.; Bolskar, R. D.; Seppelt, K.; Strauss, S. H.; Popov, A. A.; Boltalina, O. V. *J. Am. Chem. Soc.* **2006**, *128*, 15793.
(27) Cai, T.; Xu, L.; Anderson, M. R.; Ge, Z.; Zuo, T.; Wang, X.; Olmstead, M. M.; Balch, A. L.; Gibson, H. W.; Dorn, H. C. *J. Am. Chem. Soc.* **2006**, *128*, 8581.
(28) Yang, S. F.; Dunsch, L. *Chem.—Eur. J.* **2006**, *12*, 413.
(29) Kurihara, H.; Lu, X.; Iiduka, Y.; Nikawa, H.; Mizorogi, N.; Slanina, Z.; Tsuchiya, T.; Nagase, S.; Akasaka, T. *J. Am. Chem. Soc.* **2012**, *134*, 3139.
(30) Nikawa, H.; Yamada, T.; Cao, B.; Mizorogi, N.; Slanina, Z.; Tsuchiya, T.; Akasaka, T.; Yoza, K.; Nagase, S. *J. Am. Chem. Soc.* **2009**, *131*, 10950.
(31) Rodríguez-Fortea, A.; Balch, A. L.; Poblet, J. M. *Chem. Soc. Rev.* **2011**, *40*, 3551.
(32) Rodríguez-Fortea, A.; Alegret, N.; Balch, A. L.; Poblet, J. M. *Nat. Chem.* **2010**, *2*, 955.
(33) Yang, H.; Jin, H.; Zhen, H.; Wang, Z.; Liu, Z.; Beavers, C. M.; Mercado, B. Q.; Olmstead, M. M.; Balch, A. L. *J. Am. Chem. Soc.* **2011**, *133*, 6299.
(34) Yang, H.; Yu, M.; Jin, H.; Liu, Z.; Yao, M.; Liu, B.; Olmstead, M. M.; Balch, A. L. *J. Am. Chem. Soc.* **2012**, *134*, 5331.
(35) Okazaki, T.; Lian, Y. F.; Gu, Z. N.; Suenaga, K.; Shinohara, H. *Chem. Phys. Lett.* **2000**, *320*, 435.
(36) Okazaki, T.; Suenaga, K.; Lian, Y. F.; Gu, Z. N.; Shinohara, H. *J. Mol Graphics Modell.* **2001**, *19*, 244.
(37) Izuoka, A.; Tachikawa, T.; Sugawara, T.; Suzuki, Y.; Konno, M.; Saito, Y.; Shinohara, H. *Chem. Commun.* **1992**, 1472.
(38) Konarev, D. V.; Kovalevsky, A. Y.; Coppens, P.; Lyubovskaya, R. N. *Chem. Commun.* **2000**, 2357.
(39) Konarev, D. V.; Khasanov, S. S.; Saito, G.; Otsukad, A.; Lyubovskaya, R. N. *J. Mater. Chem.* **2007**, *17*, 4171.
(40) Sun, D.-Y.; Liu, Z.-Y.; Guo, X.-H.; Xu, W.-G.; Liu, S.-Y. *J. Phys. Chem. B* **1997**, *101*, 3927.
(41) Mercado, B. Q.; A. Jiang, A.; Yang, H.; Wang, Z.; Jin, H.; Liu, Z.; Olmstead, M. M.; Balch, A. L. *Angew. Chem., Int. Ed.* **2009**, *48*, 9114.
(42) Yang, H.; Jin, H.; Wang, X.; Liu, Z.; Yu, M.; Zhao, F.; Mercado, B. Q.; Olmstead, M. M.; Balch, A. L. *J. Am. Chem. Soc.* **2012**, *134*, 14127–14136.
(43) John, T.; Dennis, S.; Shinohara, H. *Appl. Phys. A: Mater. Sci. Process.* **1998**, *66*, 243.
(44) Sun, B.-Y.; Inoue, T.; Shimada, T.; Okazaki, T.; Sugai, T.; Suenaga, K.; Shinohara, H. *J. Phys. Chem. B* **2004**, *108*, 9011.
(45) Hasegawa, T.; Mochida, T.; Kondo, R.; Kagoshima, S.; Iwasa, Y.; Akutagawa, T.; Nakamura, T.; Saito, G. *Phys. Rev. B, Condens. Matter* **2000**, *62*, 10059.
(46) Konarev, D. V.; Khasanov, S. S.; Saito, G.; Otsuka, A.; Lybovskaya, R. N. *J. Mater. Chem.* **2007**, *17*, 4171.
(47) Beavers, C. M.; Jin, H.; Yang, H.; Wang, Z.; Wang, X.; Ge, H.; Liu, Z.; Mercado, B. Q.; Olmstead., M. M.; Balch, A. L. *J. Am. Chem. Soc.* **2011**, *133*, 15338.
(48) Wang, Y.-B.; Lin, Z. *J. Am. Chem. Soc.* **2003**, *125*, 6072.
(49) Pham, D.; Bertran, J. C.; Olmstead, M. M.; Mascal, M.; Balch, A. L. *Org. Lett.* **2005**, *7*, 2805.
(50) Stevenson, S.; Chancellor, C. J.; Lee, H. M.; Olmstead, M. M.; Balch, A. L. *Inorg. Chem.* **2008**, *47*, 1420.
(51) *SAINT*; Bruker AXS Inc.: Madison, WI, 2009.
(52) Sheldrick, G. M. *SADABS*; University of Göttingen: Göttingen, Germany, 2008.
(53) Sheldrick, G. M. *Acta Crystallogr.* **2008**, *A64*, 112.

(54) Dolomanov, O. V.; Bourhis, L. J.; Gildea, R. J.; Howard, J. A. K.; Puschmann, H. *J. Appl. Crystallogr.* **2009**, *42*, 229.
(55) (a) Becke, A. D. *Phys. Rev. A* **1988**, *38*, 3098. (b) Lee, C.; Yang, W.; Parr, R. G. *Phys. Rev. B* **1988**, *37*, 785.
(56) Stevens, W.; Basch, H.; Krauss, J. *J. Chem. Phys.* **1984**, *81*, 6026.
(57) Frisch, M. J.; Trucks, G. W.; Schlegel, H. B.; Scuseria, G. E.; Robb, M. A.; Cheeseman, J. R.; Montgomery, Jr., J. A.; Vreven, T.; Kudin, K. N.; Burant, J. C.; Millam, J. M.; Iyengar, S. S.; Tomasi, J.; Barone, V.; Mennucci, B.; Cossi, M.; Scalmani, G.; Rega, N.; Petersson, G. A.; Nakatsuji, H.; Hada, M.; Ehara, M.; Toyota, K.; Fukuda, R.; Hasegawa, J.; Ishida, M.; Nakajima, T.; Honda, Y.; Kitao, O.; Nakai, H.; Klene, M.; Li, X.; Knox, J. E.; Hratchian, H. P.; Cross, J. B.; Bakken, V.; Adamo, C.; Jaramillo, J.; Gomperts, R.; Stratmann, R. E.; Yazyev, O.; Austin, A. J.; Cammi, R.; Pomelli, C.; Ochterski, J. W.; Ayala, P. Y.; Morokuma, K.; Voth, G. A.; Salvador, P.; Dannenberg, J. J.; Zakrzewski, V. G.; Dapprich, S.; Daniels, A. D.; Strain, M. C.; Farkas, O.; Malick, D. K.; Rabuck, A. D.; Raghavachari, K.; Foresman, J. B.; Ortiz, J. V.; Cui, Q.; Baboul, A. G.; Clifford, S.; Cioslowski, J.; Stefanov, B. B.; Liu, G.; Liashenko, A.; Piskorz, P.; Komaromi, I.; Martin, R. L.; Fox, D. J.; Keith, T.; Al-Laham, M. A.; Peng, C. Y.; Nanayakkara, A.; Challacombe, M.; Gill, P. M. W.; Johnson, B.; Chen, W.; Wong, M. W.; Gonzalez, C.; and Pople, J. A. *GAUSSIAN 09*, Revision C.01; Gaussian, Inc.: Wallingford, CT, 2012.